Sigma J Eng & Nat Sci 37 (1), 2019, 41-70

Sigma Journal of Engineering and Natural Sciences
Sigma Mühendislik ve Fen Bilimleri Dergisi

Research Article

INCREASING THE SPEED OF FOAM INJECTION SIMULATION IN HYDROCARBON RESERVOIRS

Mehdi FOROOZANFAR*[1], Mohammad Reza RASAEI[2]

[1]*Kish International Campus, University of Tehran, IRAN;* ORCID: 0000-0002-2872-8285
[2]*Institute of Petroleum Engineering (IPE), School of Chemical Engineering, College of Engineering, University of Tehran, IRAN;* ORCID: 0000-0002-6657-5742

Received: 14.07.2018 Revised: 17.08.2018 Accepted: 19.08.2018

ABSTRACT

Reliable reservoir prediction is essential for optimized production and reservoir management. The prediction is normally done by reservoir simulation. Reservoir simulators solve fluid flow equations of reservoir numerically on homogenized coarse blocks of reservoir model. The original fine grids are generated by primary geological blocks which are output of geological software. The upscaling is necessary since geological software by means of statistical methods create models with millions and even billion of grid blocks and dynamic simulation on these models is practically not possible. In this study, we introduced different types of hybrid grid by nature-inspired method, which is the basis of scale-up model and then implement upscaling procedure. The simulation results on the geological structure well compared with the results of upscaled models. The results confirm that nature-inspired method consumes less run time with nearly accuracy of fine model.
Keywords: Foam flooding, upscaling, grid modeling, geological model, inspire, run time.

1. INTRODUCTION

Recent amelioration in reservoir imaging techniques and geostatistical procedures allow very detailed reservoir explanations containing millions of grid blocks to be produced .However, time limitations in reservoir simulation generally limit the flow model to a coarser grid. Each coarse grid block property value is received from the original fine scale grid using different upscaling techniques.

After all averaging, interpolation and data populating, from a simulation point of view, geological models are ironically too complex and too large, i.e., they contain more information than we can handle in simulation studies. Therefore, we usually use a coarsened grid model, or a simulation flow model. The model contains of grid blocks with their petrophysical properties replaced by averaged or upscaled quantities based on variations of underlying geomodel quantities that occur at length scales below the simulation grid block. The main reason for using the upscaled models is computational limitations since it is usually impossible to perform flow simulations on the geomodel. However it is worth mentioning that, the manifestation of new computers with high computational abilities gives a hope that the fine scale geological models

* Corresponding Author: e-mail: m.foroozanfar@ut.ac.ir, tel: +989190227196

will be directly used for flow simulation. To this hope one must notice that the sizes and complexity of geomodels have been increasing continuously and simultaneously with the growth of computer memory and processing power. Therefore, considering this current trend, the upscaling of geomodels seems an unavoidable stage of reservoir studies (Masoud,Babaei, 2013).

In the upscaling techniques that coarsen the geomodels to simulation models, the effective petrophysical properties are calculated in each cell of the simulation grids based on properties of the underlying geomodels. In this process, the target is to maintain as much as possible the small scale effects in the large scale calculations. Systematic small scale alterations in permeability and porosity can have a considerable effect on a larger scale, and this should be captured in the upscaled model. The quality of upscaling is usually assessed by comparing upscaled production characteristics with those obtained from a reference solution computed on an underlying fine grid (Aarnes *et al.*, 2007). The closer the production predictions of an upscaling technique for a reservoir model is to those received by the fine scale reference model, the better the upscaling technique is rendered(M.Babaei, 2013).

Upscaling techniques are mainly classified into single phase and multiphase flow upscaling methods. In multiphase flow upscaling, the problem is to upscale relative permeabilities and capillary pressure, that exist only for multiphase flow, in addition to absolute permeability and porosity. Reviews on single phase flow upscaling can be found for example in Renard & de Marsily (1997) and Farmer (2002). Reviews on multiphase flow upscaling can be found in Barker & Thibeau (1997) and Das & Hassanizadeh (2005) (M,Babaei 2013).

For upscaling multiphase flow, in addition to absolute permeabilities, relative permeabilities should be upscaled. Therefore, it is necessary to express the saturation equation in coarse scale. One way to write an upscaled saturation equation is by assuming that the functional form of these properties does not change with scale. In this case the same relative permeability and capillary pressure curves from fine to coarse scale are used. Unfortunately this suggestion fails in the presence of non-local heterogeneities similar to failure in the case of absolute permeability upscaling. In these circumstances, a multiphase upscaling technique is generally required (Barker & Thibeau, 1997) (M. Babaei,2013).

The objective of this paper is to define inspired by nature upscaling method for a 3D heterogeneous multiphase reservoir. Using the IMPES and fully implicit as solver methods. The new techniques are used in this study utilization of unstructured gird in order to hybrid grid simulation for instance, composite grid consisting of a regular Cartesian mesh with radial refinement around well positions and defined upscaling methods for different terms like absolute permeability, relative permeability, transmissibility, pore volume and some foam flooding properties.

2. GRID MODELING (GRID TYPES)

2.1. Structured Grids

A grid is a tessellation of a planar or volumetric object by a set of simple shapes. In a structured grid, only one basic shape is allowed and this basic shape is laid out in a regular repeating pattern so that the topology of the grid is constant in space. The most typical structured grids are based on quadrilaterals in 2D and hexahedrons in 3D, but in principle it is also possible to construct grids with a fixed topology using certain other shapes. Structured grids can be generalized to so-called multi block grids (or hybrid grids), in which each block consists of basic shapes that are laid out in a regular repeating pattern.[3]

2.1.1. Regular Cartesian Grids

The simplest form of a structured grid consists of unit squares in 2D and unit cubes in 3D, so that all vertices in the grid are integer points. More generally, a regular Cartesian grid can be defined as consisting of congruent rectangles in 2D and rectilinear parallelepipeds in 3D, etc.[3]

2.1.1.1. Rectil inear Grids

A rectilinear grid (Figure 1) (also called a tensor grid) consists of rectilinear shapes (rectangles or parallelepipeds) that are not necessarily congruent to each other. In other words, whereas a regular Cartesian grid has a uniform spacing between its vertices, the grid spacing can vary along the coordinate directions in a rectilinear grid.[3]

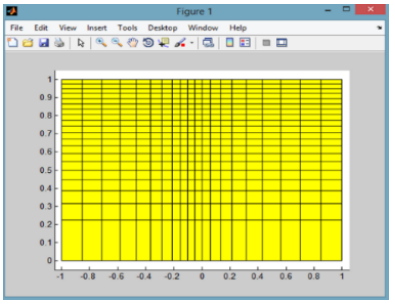

Figure 1. Example of a Rectilinear Grid

2.1.1.2. Curvilinear Grids

A curvilinear grid is a grid with the same topological structure as a regular Cartesian grid, but in which the cells are quadrilaterals rather than rectangles in 2D and cuboids rather than parallelepipeds in 3D. The grid is given by the coordinates of the vertices (Figure 2).[3]

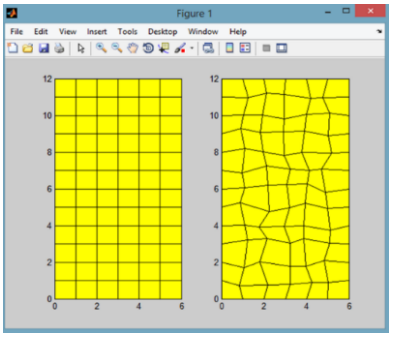

Figure 2. Example of Curvilinear Grids

2.2. PEBI† Grids

PEBI grids are often used to overcome the problem of areal adaption. These grids have been designed to combine the advantages of two different gridding methods: the flexibility of unstructured grids and the orthogonality of Cartesian grids. The PEBI grids are constructed in much of the same way as corner-point grids. One can, for instance, start with a point set, generate a lateral along one or more horizons, construct a lateral polyhedral grid by connecting the perpendicular bisectors of the triangle edges, one define a set of pillars that align with the major faults, and use these to extrude the areal grid cells to a volumetric grid (Figure 3).[4]

† Perpendicular Bisector

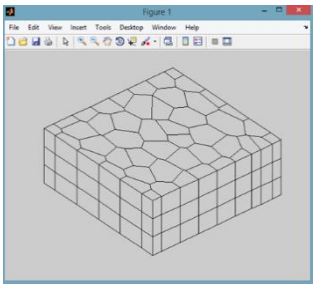

Figure 3. Example of PEBI Grids

2.3. Radial Grids

To simulate in radial coordinate system, we need the following specialized information:

DIMENS: In the radial case, this term specifies the number of cells in the r, θ and z directions.

INRAD: Specify inner radius of first grid block in the radial direction.

DRV: Specify grid block dimensions in the R directions.

DTHETA: Size in the theta (θ) direction.

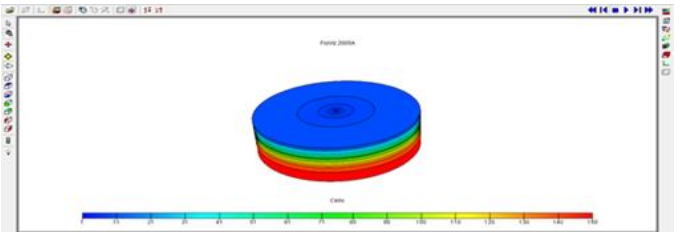

Figure 4. Example of Radial Grid

2.4. Composite Grids

One advantage of an unstructured grid description is that it easily allows the use of composite grids consisting of geometries and topologies that vary throughout the model. That is, different grid types or different grid resolution may be used locally to adapt to well trajectories and special features in the geology.[2]

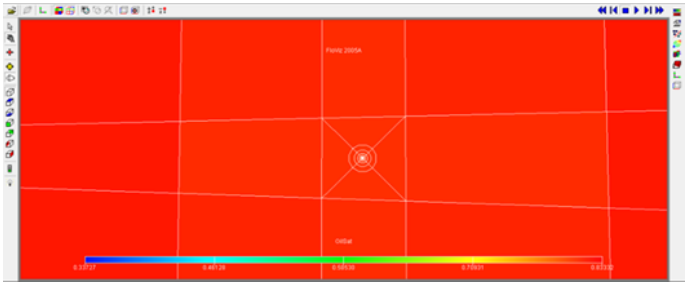

Figure 5. Composite Grid Consisting of a Regular Cartesian Mesh with Radial Refinement around Well Positions

3. UPSCALING METHOD, INSPIRED BY NATURE (UPIN) (UPSCALING PATTERN, STRUCTURE METHOD)

The division of the Earth's surface is done by the latitude and longitude of the planet this kind of division is the inspirational basis for increasing the scale.

- Latitude: Lines of latitude called parallels, measure distance north and south of equator.
- Longitude: Lines of longitude called meridians, measure distance east and west of prime meridian.

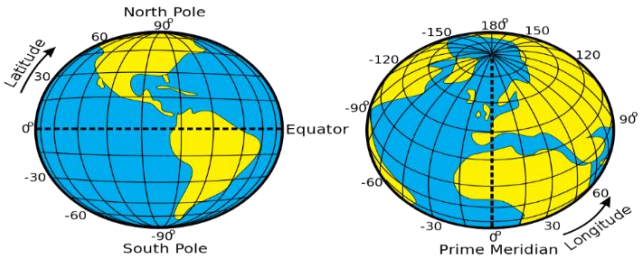

Figure 6. Latitude and Longitude

According to the figure 6:
Latitude ≈ Discretization in Y direction in simulation model
Longitude ≈ Discretization in X direction in simulation model

The earth grid in the north and South Pole and in the equator is in the following form:

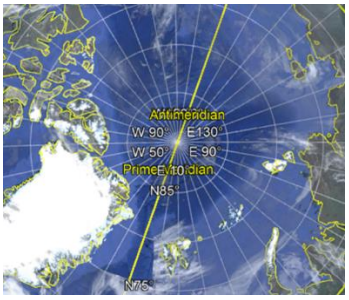

Figure 7. Grid Earth in the North Pole (Fine and Radial Form)

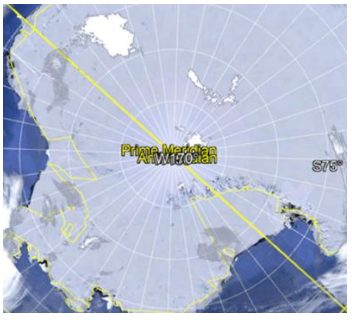

Figure 8. Grid Earth in the South Pole (Fine and Radial Form)

Figure 9. Grid Earth in the Equator (Coarse and Cartesian Form)

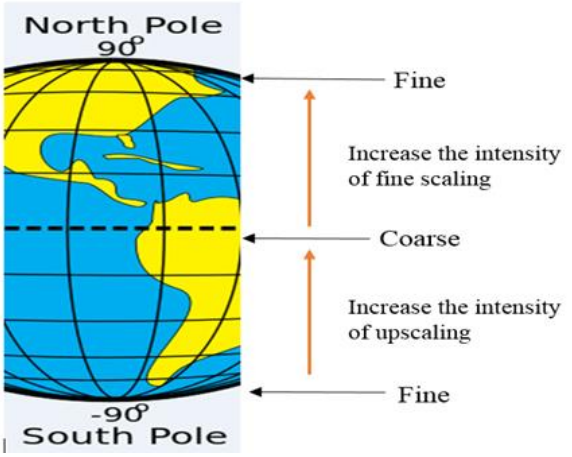

Figure 10. Size Change of Grid Earth

According to the figures 7, 8 and 9 grid earth is in the form of hybrid grid.
Now looking for the similarity of the planet with a reservoir, look at the figure below:

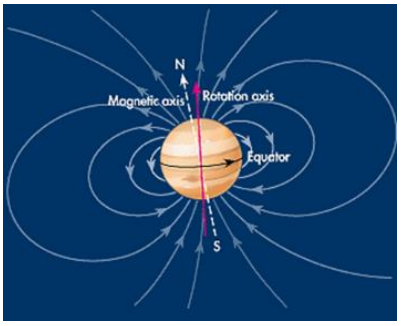

Figure 11. Earth's Magnetic Field

According to figure 11:
North Pole ≈ Production Well
South Pole ≈ Injection Well
Earth's Magnetic Field≈ Stream Lines in a Reservoir

The principle of scaling up is, important areas such as wellbore or existence of fracture in the reservoir remain fine scale and features that these areas have cause to converge the stream lines and distance between them reduced (figure 12,13).

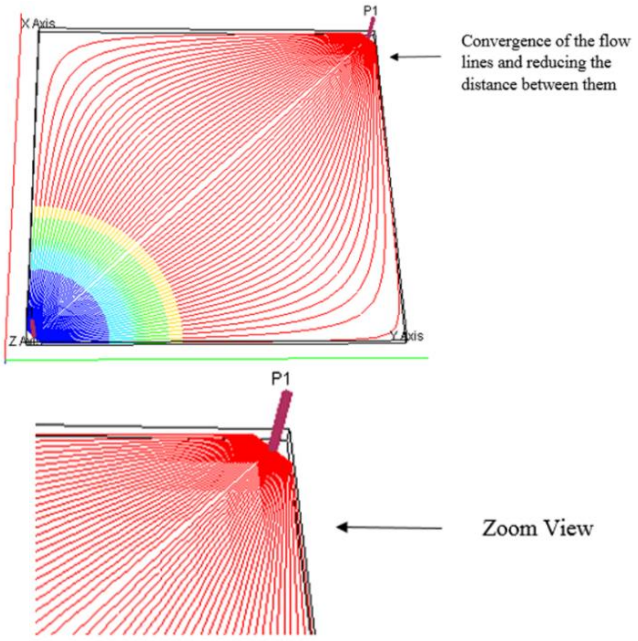

Figure 12. Convergence of Flow Lines around the Wellbore

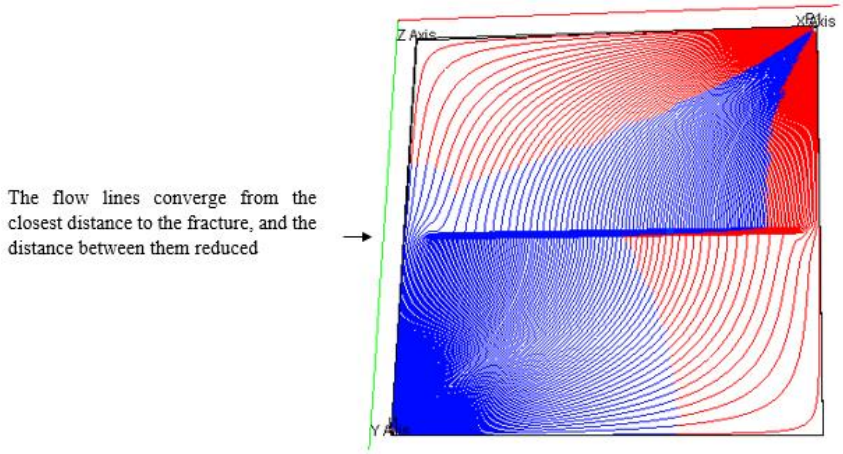

Figure 13. Convergence of Flow Lines around the Fracture

4. INTRODUCTION OF STUDIED RESERVOIR

The Reservoir has the following properties:

A 3D case with a fine mesh composed of $[40 \times 40 \times 3]$ (Total cell number: 4800). The permeability field is a distribution of high and a low values, 100 and 5 md, respectively. The porosity is constant and equal to 0.3 and in the fractured reservoir study fracture permeability is 300 md and SIGMA value is 0.0108, initial reservoir pressure is 4,800 psi.

Table 1. Water Properties

	Reference Pressure(psi)	Water Formation Volume Factor(bbl/STB)	Water Compressibility	Water Viscosity(cP)
PVTW	4014.7	1.029	3.13E-06	0.31

Table 2. Rock Properties

	Reference Pressure(psi)	Rock Compressibility	Porosity
Rock	14.7	3.0E-06	0.3

Table 3. Surface Densities of Reservoir Fluids

	Oil	Water	Gas
Surface Densities of Reservoir Fluids ($\frac{lb}{ft^3}$)	49.1	64.79	0.06054

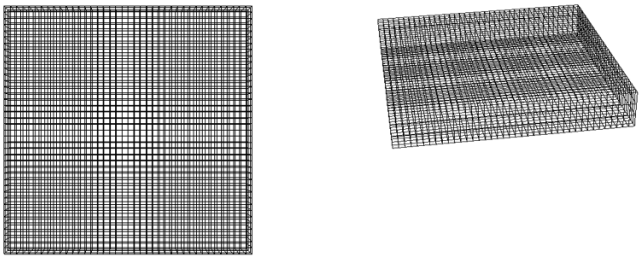

Figure 14. Fine Model of the Reservoir

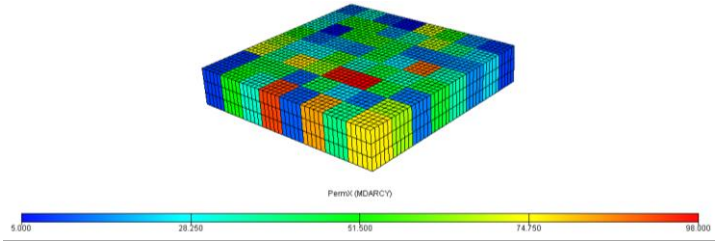

Figure 15. Permeability Map, Reservoir Dimension $[40 \times 40 \times 3]$

5. FOAM FLOODING SIMULATION

Foam can be used in a number of ways to increase the production from an oil reservoir. The foam acts to decrease the mobility of gas; this effect can be used to slow the breakthrough of injected gas or to reduce the production of gas cap gas.

A foam is generated by adding a surfactant to an aqueous phase, and passing a gas through the surfactant to generate stable dispersion of gas bubble in the liquid. The foam can be transported with the gas flow into the reservoir. The reduction of gas mobility typically depends on a range of factors including pressure and shear rate.

The foam stability has a major effect on the usefulness of foam injection. Typically the foam suffers from adsorption on to the rock matrix, decay over time, and enhanced decay in the presence of water and oil. The adsorption of foam is assumed to be instantaneous, and the

quantity adsorbed is a function of active foam concentration. I am required to supply an adsorption isotherm as a function of foam concentration.

5.1. The Quantity of Foam Adsorbed on the Rock is Given By:

$$\text{Mass of adsorbed foam} = PV.\left(\frac{1-\emptyset}{\emptyset}\right).\rho_r.\text{CA}(C_{foam}) \quad (1)$$

Where

PV: is the pore volume of the cell
$\emptyset$: is the porosity
ρ_r: is the mass density of the rock
$CA(C_{foam})$: is the adsorption isotherm as a function of local foam concentration in solution

5.2. Foam Decay

Foam effectiveness will typically reduce over time, even in conditions very favorable to foam stability. This reduction in effectiveness may be accelerated in the presence of water or oil. The reduction in foam effectiveness over time is modeled by foam decay that is function of both oil and water saturation.

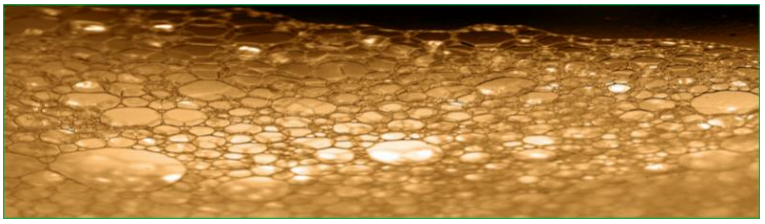

Figure 16. Foam Flooding

5.3. Gas Mobility Reduction

The foam modifies the gas mobility by way of simple multiplier as a function of foam concentration (that is the effective surfactant concentration).

$$\text{Unmodified gas flow: } F_g = \frac{K_{rg}}{\mu_g B_g}(T.DP) \quad (2)$$

$$\text{Modified flow: } f_{gm} = M(C_{foam})\frac{K_{rg}}{\mu_g B_g}(T.DP) = M(C_{foam})F_g \quad (3)$$

K_{rg}: is the gas relative permeability
μ_g: is the gas viscosity
B_g : is the gas formation volume factor
T: is the transmissibility
DP: is the pressure difference
$M(C_{foam})$: is the input mobility reduction factor
C_{foam} : is the foam concentration

The mobility reduction factor $M(C_{foam})$ influenced by two separate effects , both of which will tend to increase M(gas mobility) , the first is pressure and the second is shear rate.

5.4. The Mobility Reduction Factor Including the Pressure Effect is:

$$MP= (1-M(C_{foam}))M_P(P) + M(C_{foam}) \quad (4)$$

Where

MP: is the mobility reduction factor with the pressure effect
$M(C_{foam})$: is the original reduction factor as a function of foam concentration
M_P(P): is the pressure dependency function
P: is the oil pressure

5.5. The Mobility Reduction Factor Including the Shear Effect is:

$$MF= (1-MP)M_s(v) + MP \quad (5)$$

Where

MF: is the final mobility reduction factor
MP: is the mobility reduction factor after applying pressure effect
M_s(v) : is the shear dependency function
V: is the gas velocity

The gas velocity is calculated as:

$$V=B_g\left(\frac{F_g}{\emptyset.A}\right) \quad (6)$$

Where

F_g: is the gas flow rate
B_g: is the gas formation volume factor
$\emptyset$: is the average porosity of cell
A: is the flow area

Table 4. Foam Adsorption Function

The Local Foam Concentration in the Solution Surrounding the Rock(lb/STB)	The Corresponding Saturated Concentration of Foam Adsorbed by the Rock Formation(lb/lb)
0.0	0.0
1.0	0.00005
30.0	0.00005
0.0	0.0
1.0	0.00002
30.0	0.00002

Table 5. Foam Decay Data as a Function of Water Saturation

The Local Water Saturation	The Corresponding Decay Half-Life(Days)
0.0	3,000
1.0	2,000
0.0	3,000
1.0	2,000

Table 6. Foam Decay Data as a Function of Oil Saturation

The Local Oil Saturation	The Corresponding Decay Half-Life(Days)
0.0	3,000
1.0	2,500
0.0	3,000
1.0	2,500

Table 7. Gas Mobility Reduction Data

The Foam Concentration(lb/STB)	The Corresponding Gas Mobility Reduction Factor
0.0	1.0
0.001	0.4
0.1	0.1
1.2	0.05

Table 8. Specifies the Foam-Rock Properties

The Adsorption Index	The Mass Density of The Rock Type at Reservoir Conditions ($\frac{lb}{rft^3}$)
1	2,650

Table 9. Pressure Dependence of Foam Mobility Reduction

The Oil Phase Pressure (Psia)	The Corresponding Pressure Modifier on the Foam Mobility Reduction Factor
3,000	0.0
6,000	0.2

Table 10. Shear Dependence of Foam Mobility Reduction

The Gas Phase Flow Velocity (ft/day)	The Corresponding Shear Modifier on The Foam Mobility Reduction Factor
0.0	0.0
4.0	0.1

6. THE PROCEDURE OF UPSCALING

Now we are going to define the methods used for upscaling for various parameters.

6.1. Grid Block Size

Within each coarse block the properties are simply upscaled from fine (f) to coarse (c) in a single coarse cell amalgamation $(I1, I2) \times (J1, J2) \times (K1, K2)$ as follows:

$$DX_c = \frac{\sum_f DX_f}{(J_2 - J_1 + 1)(K_2 - K_1 + 1)} \tag{7}$$

$$DY_c = \frac{\sum_f DY_f}{(I_2 - I_1 + 1)(K_2 - K_1 + 1)} \tag{8}$$

$$DZ_c = \frac{\sum_f DZ_f}{(I_2 - I_1 + 1)(J_2 - J_1 + 1)} \tag{9}$$

Where

c: Coarse
f: Fine

6.2. Renormalization Method (Upscaling For Absolute Permeability):

A way to calculate **k** is the renormalization method for 2 or 3D case studies. Renormalization is a recursive algorithm. The effective properties of small regions of the reservoirs are first calculated and then placed on a coarse grid. The grid is further coarsened and the process repeated until a single effective property has been calculated (King et al., 1993). The renormalization transformation is by no means unique and many different renormalization schemes have been proposed, some inspired by an analogy between flow in porous media, percolation processes and the flow of currents through resistors (King, 1989).

$$\mathbf{K} = f(K_1, K_2, K_3, K_4) \tag{10}$$

$$f = \frac{(2(K_1+K_2)(K_3+K_4)(K_{12}+K_{34}))}{3(K_1+K_3)(K_2+K_4)+\frac{1}{2}(K_1+K_2+K_3+K_4)(K_{12}+K_{34})} \tag{11}$$

Where

K_1, K_2, K_3, K_4: Absolute permeabilities of four constituent fine cells
K_{12}, K_{34}: Harmonic means of permeabilities of the cells with the given subscripts

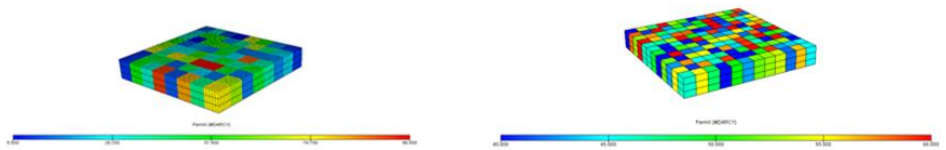

Absolute Permeability Range (MDarcy): 5-100
Dimension: [40 × 40 × 3]

Absolute Permeability Range (MDarcy): 40-60
Dimension: [12 × 12 × 3]

Figure 17. Implementation the Procedure of Upscaling For Absolute Permeability (Static Model)[12 × 12 × 3]

We should avoid defining too large coarse cells in order to encompass wide relative permeability variations between different rock types.

6.3. Pseudo-Function Generation:

For single phase flow, permeability is assumed to be a rock property and independent of the fluids present. This is only true in the case where the rock is completely saturated with a specific fluid. In the case where two fluids are present, it is necessary to define phase specific permeabilities which are defined as the product of the absolute permeability of the rock and a function of saturation of the phase considered. Relative permeabilities are functions of saturation, implying that in the presence of more than one phase in the rock, an equation for saturation will also be needed. Assuming that a generalization of Darcy's law to multiphase flow is valid (Bear, 1972), we need to formulate equations for the flow of each phase l using relative permeabilities:

$$V_l = -\frac{\mathbf{K}K_{rl}(S_l)}{\mu_l}(\nabla p_l + \rho_l g \nabla z) \quad (12)$$

Where

V: Volumetric flow
p: Pressure
g: Gravitational Force
z: Spatial coordinate

A common approach is to use an averaging technique to generate relative permeability curves similar to global-local upscaling. For instance, for calculating an upscaled mobility of phase l, denoted by λ_l^* , a fine scale global solution, provides the flow rate between the grid blocks. To match the phase flow rates between coarse grid blocks E_i and E_j in *x* direction the following must hold:

$$\sum_{K=1}^{N}(f_l)_k = \overline{f}_l \quad (13)$$

Substituting in Darcy's law for multiphase flow:

$$-\sum_{K=1}^{N}(t\lambda_l(S)\nabla p)_K = -(T^*\lambda_l^*(\overline{S})\nabla\overline{p})_{ij} \quad (14)$$

Where

t: Fine transmissibility
T^*: Coarse transmissibility

The upscaling for transmissibilities is achieved as a simple average. Between the centers of two neighboring coarse cells, $TRANX_C$ $(Coarse\ transmissibility\ in\ X-direction)$is obtained from a harmonic average of $TRANX_f(Fine\ transmissibility\ in\ X-direction)$in the X-direction and by summing in the Y- and Zdirections so that:

$$TRANX_c = \sum_J \sum_K \left[\frac{1}{\sum_I \left[\frac{1}{TRANX_f}\right]}\right]$$

6.4. Pore Volume Averaged Equations

The pore volume of a refined global cell may differ from the sum of the pore volumes of the local cells which it contains, either because the local porosities and net-to-gross ratios differ from the values for the host cell or because of discrepancies in geometry. After computing the local pore volumes, replaced the pore volume of the host cell with the sum of the refined pore volumes.

$$PV_{cx} = \frac{\sum_f PV_f Kx_f}{Kx_c}$$

$$PV_{cy} = \frac{\sum_f PV_f Ky_f}{Ky_c}$$

$$PV_{cz} = \frac{\sum_f PV_f Kz_f}{Kz_c}$$

c: Coarse
f: Fine
PV: Pore Volume

$$PV_c = \sum_f PV_f$$

6.5. Upscaling For Foam Adsorbed on the Rock:

In the equation of mass of adsorbed foam there is a term that in the case of different rock types need to define upscaling method, mass density of the rock (ρ_r). Figure 16 shows the mass density range for different rock types. (we consider porosity is constant through the reservoir).

$$\text{Mass of adsorbed foam} = PV.\left(\frac{1-\emptyset}{\emptyset}\right).\rho_r.\text{CA}(C_{foam}) \quad (15)$$

Where

PV: is the pore volume of the cell
$\emptyset$: is the porosity
ρ_r: is the mass density of the rock
$CA(C_{foam})$: is the adsorption isotherm as a function of local foam concentration in solution

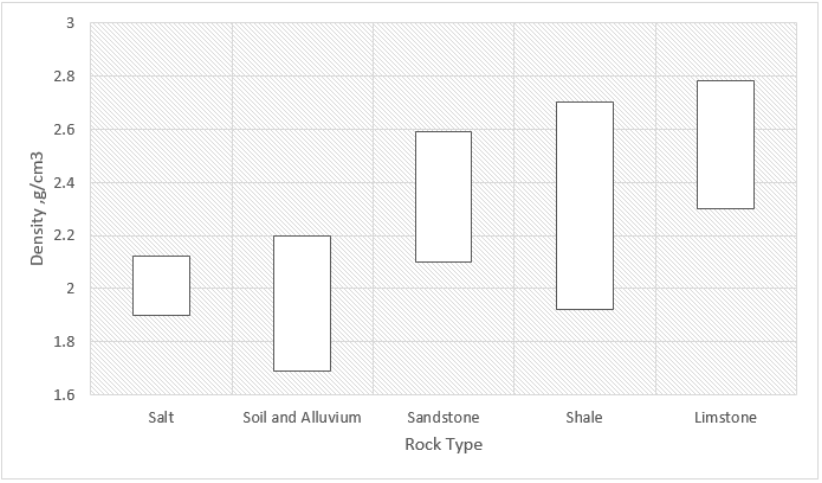

Figure 18. Mass Density of Different Rock Types

$$\text{Mass of adsorbed foam (Upscaled)} = PV.\left(\frac{1-\emptyset}{\emptyset}\right).\frac{\sum\rho_r}{n}.\text{CA}(C_{foam}) \quad (16)$$

7. TEST CASES:

In this section, different cases like diagonal and 5-spot well pattern and a fractured reservoir are presented to test the inspired by nature upscaling approach.

7.1. Reservoir with one Injection and Production Well (Diagonal Pattern)

The first case show in this study corresponds to a 3D case with a fine mesh composed of 40 by 40, 4800 cells with three layers and a coarse mesh of 12 by 12 cells (Figure 19). The range of permeability field is a distribution of high and a low values, 100 and 5 md (for fine model), respectively and for upscaled model 60 (high) and 40 (low) md . The porosity is constant and equal to 0.3. Gas is injected at one corner of the model at a rate of 100,000 Mscf/day, and the fluid is produced at the opposite corner. The concentration of foam in the injection stream for injection well is 1.1 lb/STB. Simulation Duration, 7110 Days.

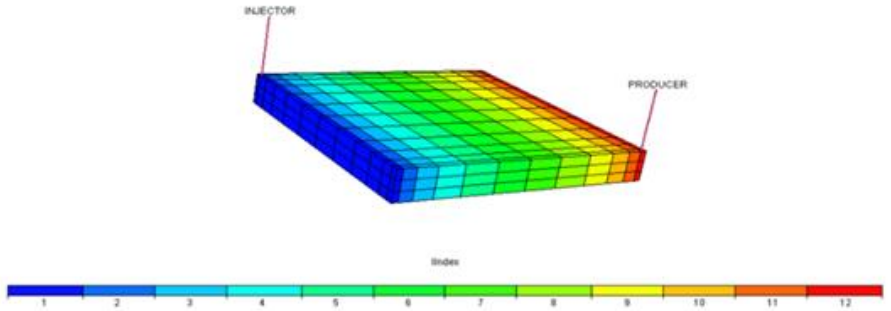

Figure 19. Upscaled view of a Reservoir with one Injection and Production Well

7.2 5-Spot Pattern

The second case showed in this study corresponds to a 3D case with a fine mesh composed of 40 by 40 , 4800 cells with three layers and a coarse mesh of 16 by 16 cells (Figure 20). The range of permeability field is a distribution of high and a low values, 100 and 5 md (for fine model), respectively and for upscaled model 60 (high) and 40 (low) md . The porosity is constant and equal to 0.3. Gas is injected at four corners of the model at a rate of 5,000 Mscf/day for each injection well, and the fluid is produced at the center of model. The concentration of foam in the injection stream for injection well is 1 lb/STB for each injection well. Simulation Duration, 2610 Days.

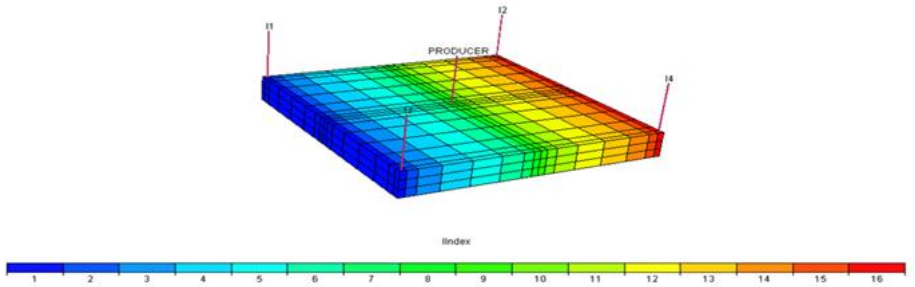

Figure 20. Upscaled view of a Reservoir with 5-Spot Pattern

7.3. Fractured Reservoir

The third case showed in this study corresponds to a 3D case with a fine mesh composed of 40 by 40, 4800 cells with three layers and a coarse mesh of 12 by 12 cells (Figure 21). The range of permeability field is a distribution of high and a low values, 100 and 5 md (for fine model), respectively and for upscaled model 60 (high) and 40 (low) md and fracture permeability is 300 md and SIGMA value is 0.0108. The porosity is constant and equal to 0.3. Gas is injected at one corner of the model at a rate of 100,000 Mscf/day, and the fluid is produced at the opposite corner. The concentration of foam in the injection stream for injection well is 1.1 lb/STB. Simulation Duration, 7110 Days.

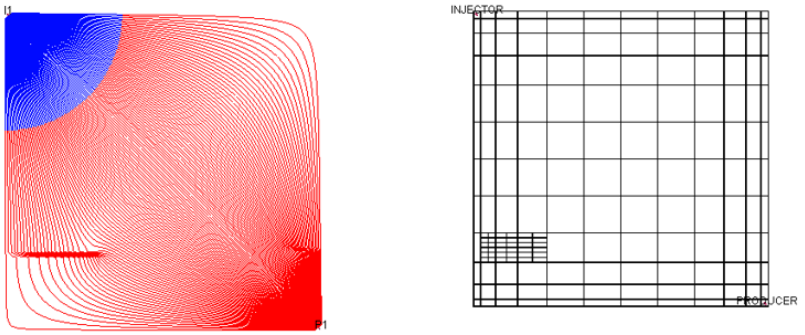

Figure 21. Upscaled View of Fractured Reservoir

Figures 22 and 23 clarify schematically different well-pattern.

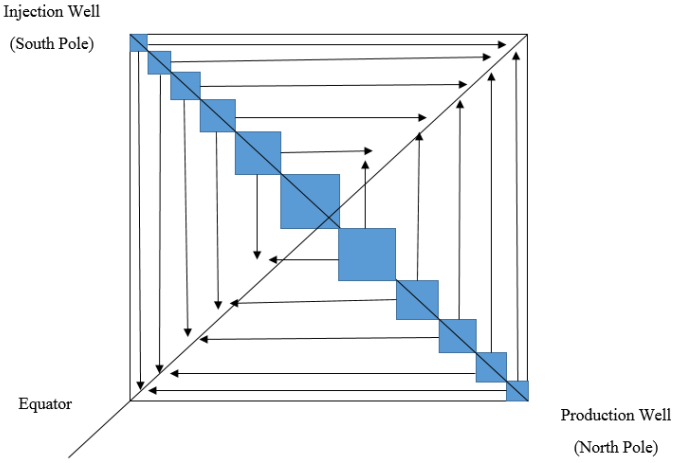

Figure 22. UPIN Pattern for a Reservoir with one Injection and Production Well

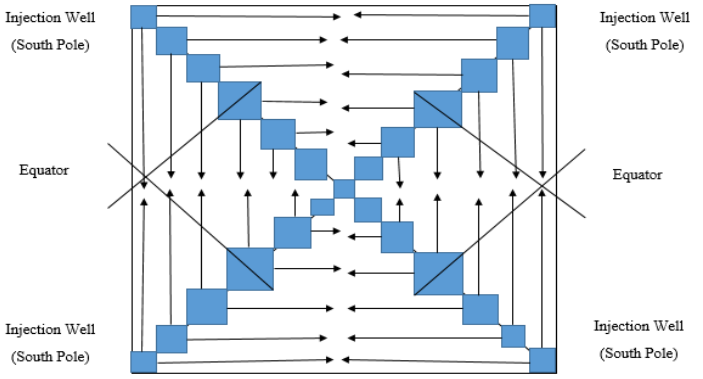

Figure 23. UPIN Pattern for 5-Spot Well Design

8. NUMERICAL RESULTS AND DISCUSSION

In this section we investigated the result of method defined previous .The different scenarios defined as below:

- **Fine Model:** Fine and heterogeneous model with 3 layers and 4800 cells.
- **UPIN:** A multiphase upscaling method which inspired by grid Earth and able to identify places with high permeability based on the behavior of flow lines (frontsim) and perform in each layer in vertical direction.
- **UPIN(CW),UPIN(RW):** In order to enhance resolution around significant regions in different geometries (Cartesian and Radial) these scenarios defined.(Transmissibility calculations in different geometries explained in appendix).

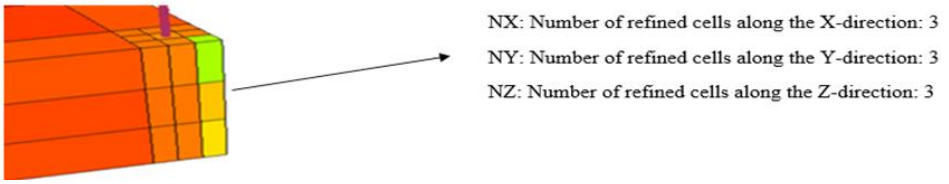

Figure 24. Local Grid Refinement (LGR) around the Production Wellbore in Cartesian Coordinate, UPIN(CW), Increasing the Resolution around the Production Well For Diagonal Pattern

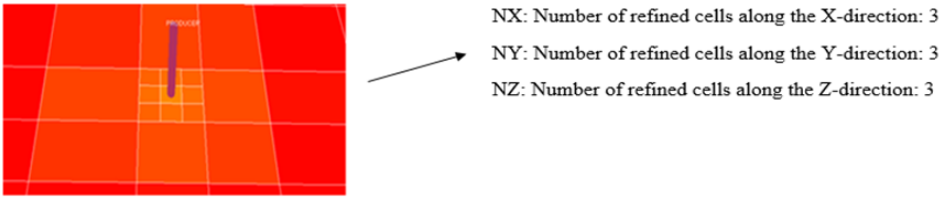

Figure 25. Local Grid Refinement (LGR) around the Production Wellbore in Cartesian Coordinate, UPIN(CW), Increasing the Resolution around the Production Well For Diagonal Pattern For 5-Spot Pattern

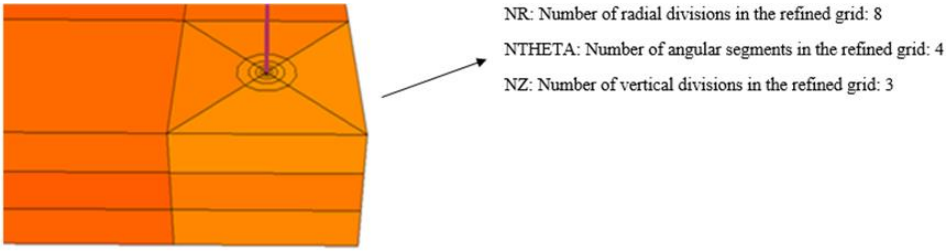

Figure 26. Local Grid Refinement (LGR) around the Production Wellbore in Radial Coordinate (Hybrid Grid), UPIN (RW), Increasing the Resolution around the Production Well For Diagonal Pattern

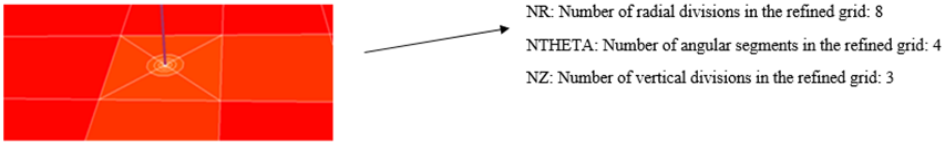

Figure 27. Local Grid Refinement (LGR) around the Production Wellbore in Radial Coordinate (Hybrid Grid), UPIN (RW), Increasing the Resolution around the Production Well For 5-Spot Pattern

First of all need to choose the solver method (Fully Implicit or IMPES) for fine model and choose one of them base on minimum elapse time, in three different cases we investigated fully implicit was faster enough in compare with IMPES method therefore, we selected fully implicit as our solver method.

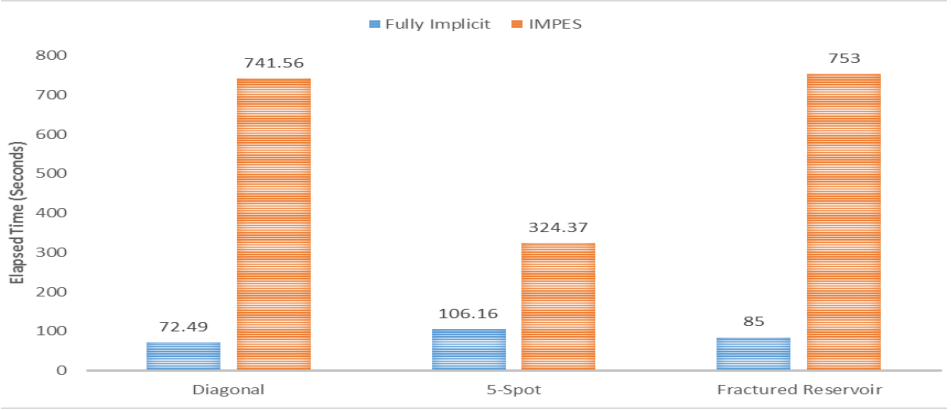

Figure 28. Elapsed Time For Fine Model in Two Different Methods

8.1. Reservoir with one Injection and Production Well (Diagonal Pattern)

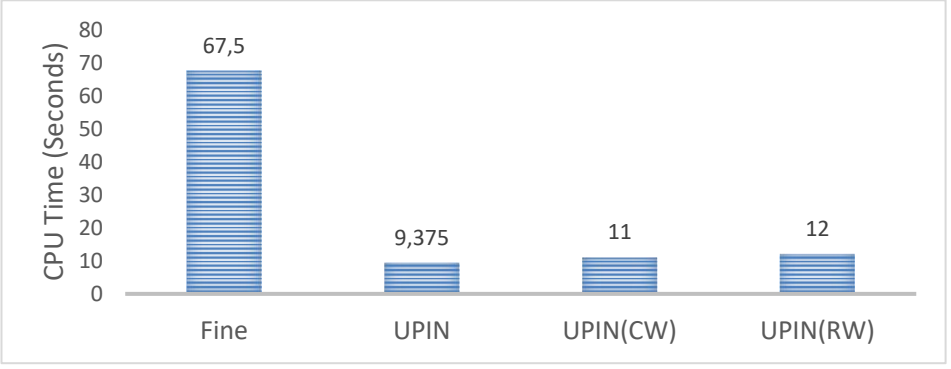

Figure 29. CPU Time for Diagonal Pattern

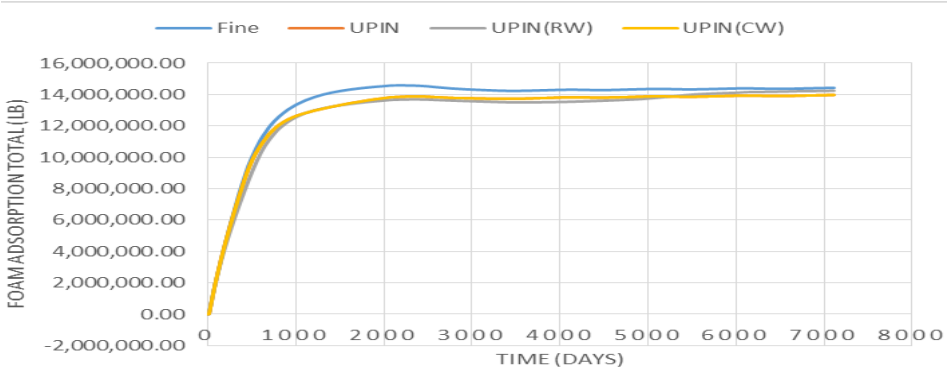

Figure 30. Foam Adsorption Total for Diagonal Pattern

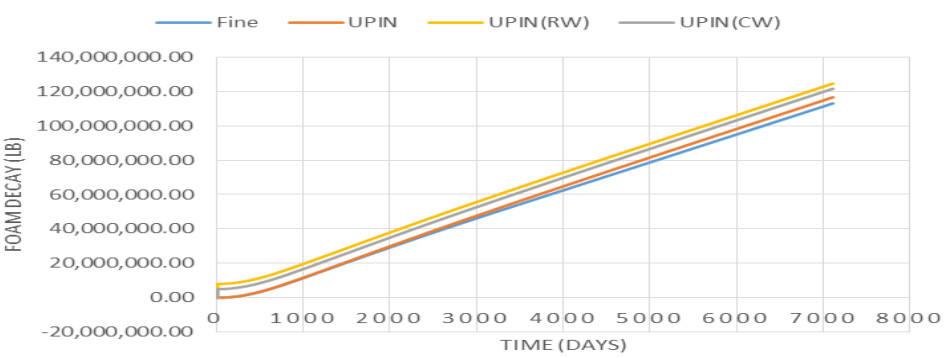

Figure 31. Foam Decay for Diagonal Pattern

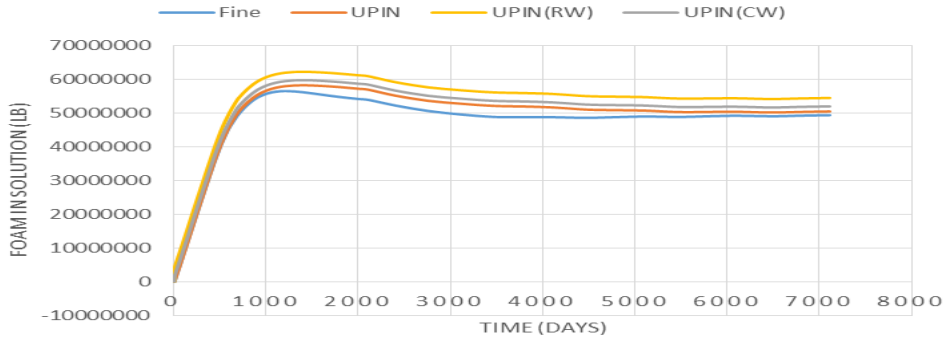

Figure 32. Foam in Solution for Diagonal Pattern

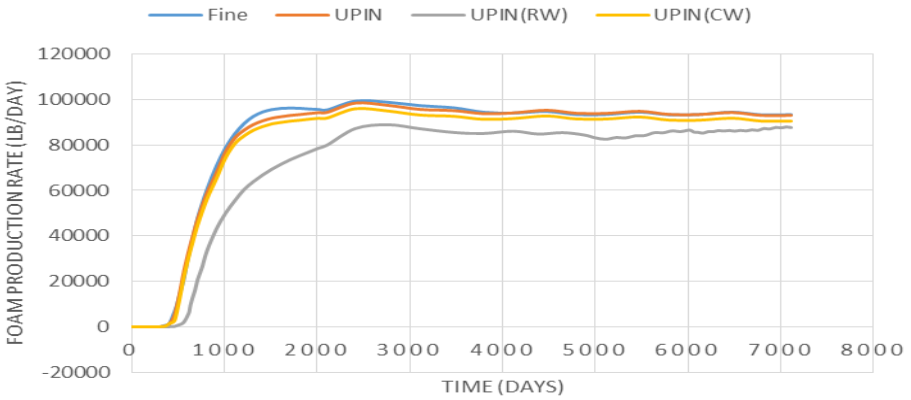

Figure 33. Foam Production Rate for Diagonal Pattern

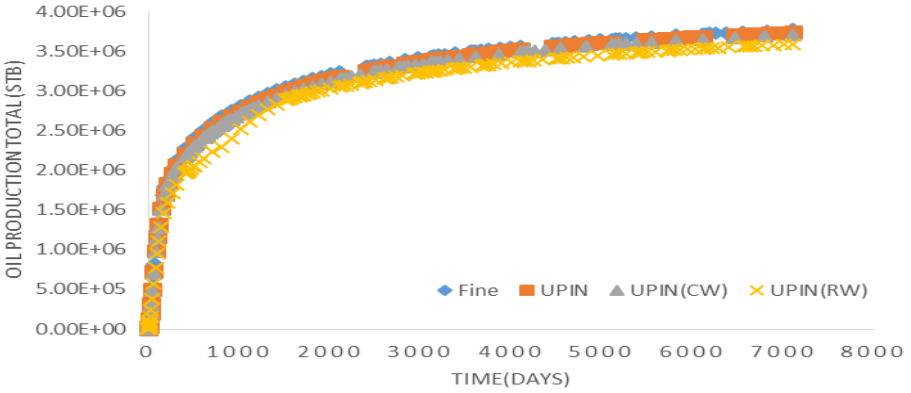

Figure 34. Oil Production Total for Diagonal Pattern

8.2 5-Spot Pattern

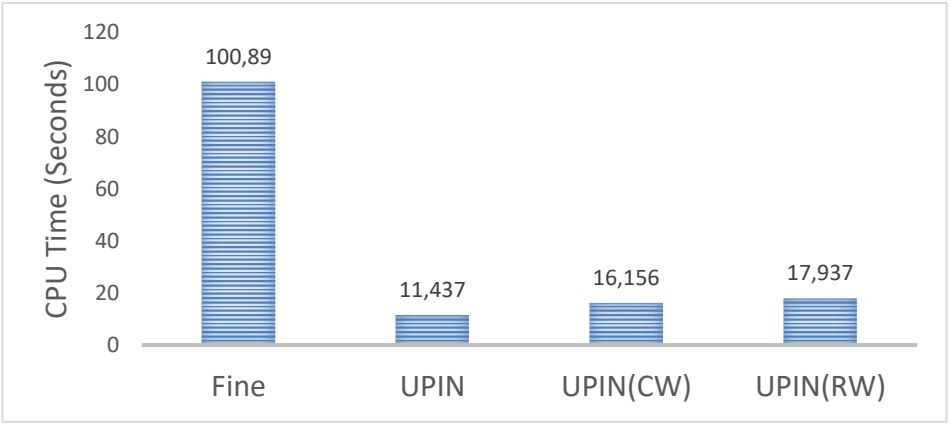

Figure 35. CPU Time for 5-Spot Pattern

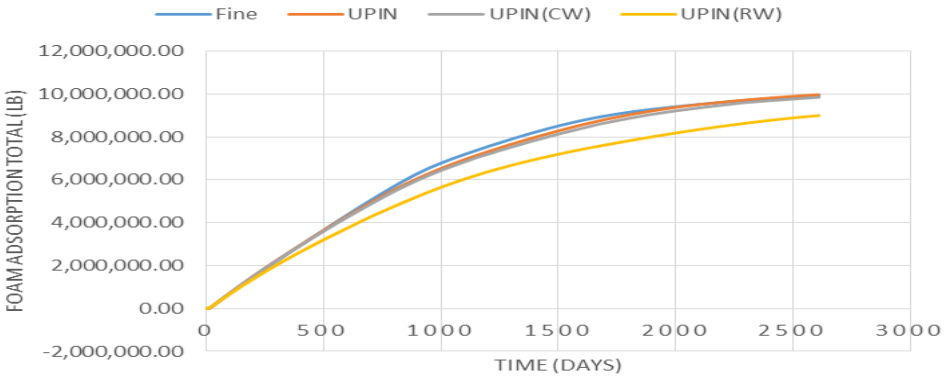

Figure 36. Foam Adsorption Total for 5-Spot Pattern

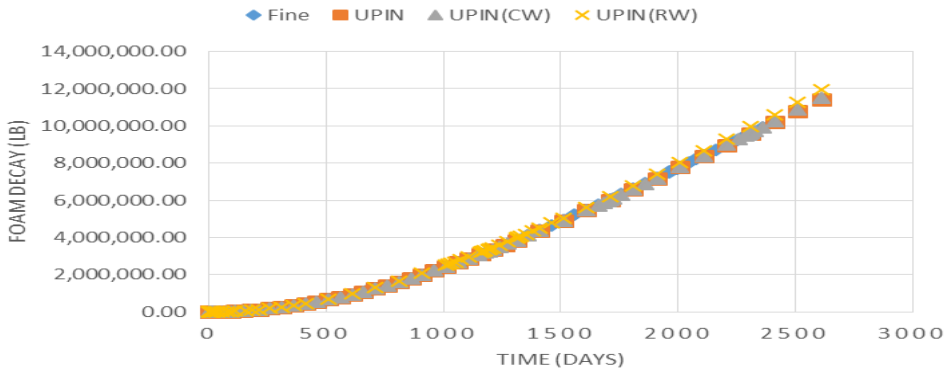

Figure 37. Foam Decay for 5-Spot Pattern

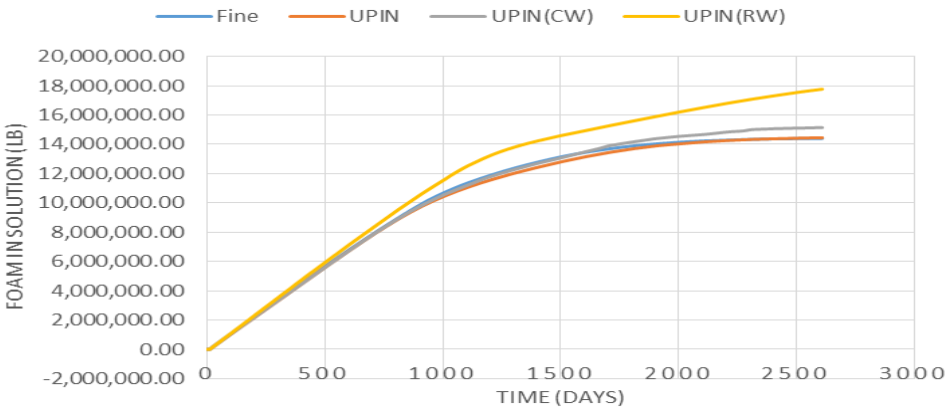

Figure 38. Foam in Solution for 5-Spot Pattern

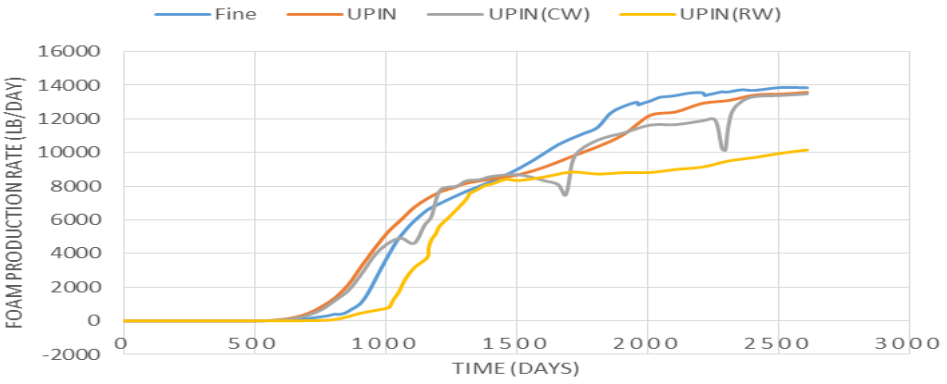

Figure 39. Foam Production Rate for 5-Spot Pattern

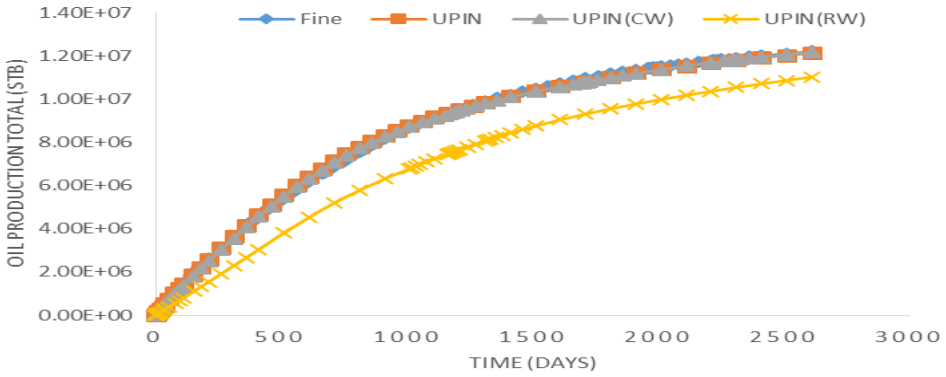

Figure 40. Oil Production Total for 5-Spot Pattern

8.3. Fractured Reservoir

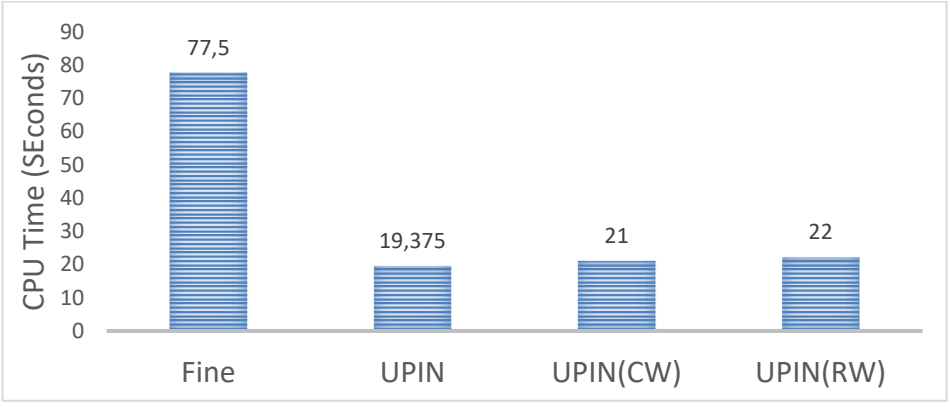

Figure 41. CPU Time for Fractured Reservoir

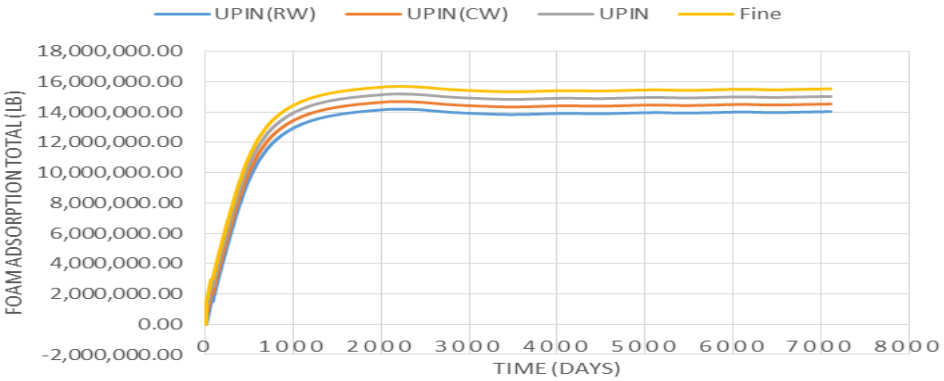

Figure 42. Foam Adsorption Total for Fractured Reservoir

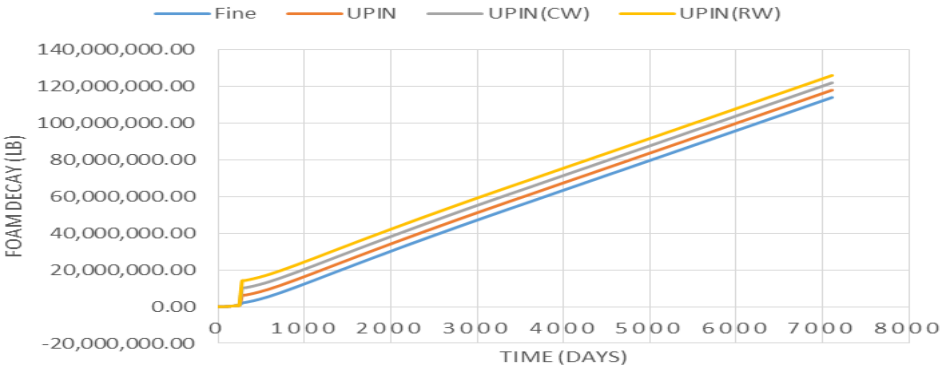

Figure 43. Foam Decay for Fractured Reservoir

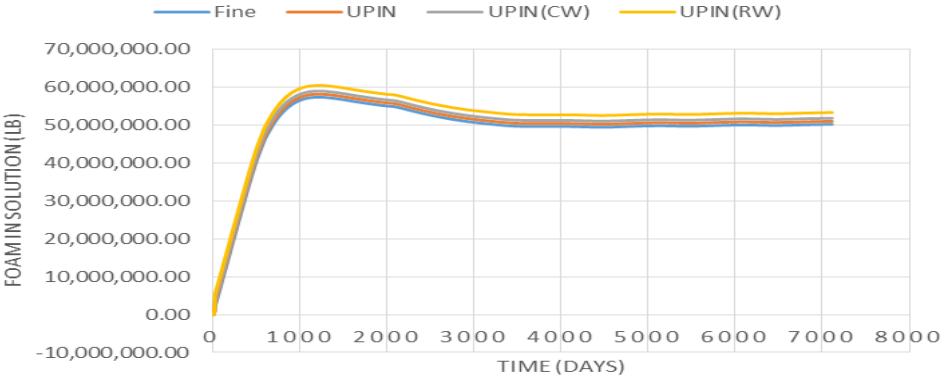

Figure 44. Foam in Solution for Fractured Reservoir

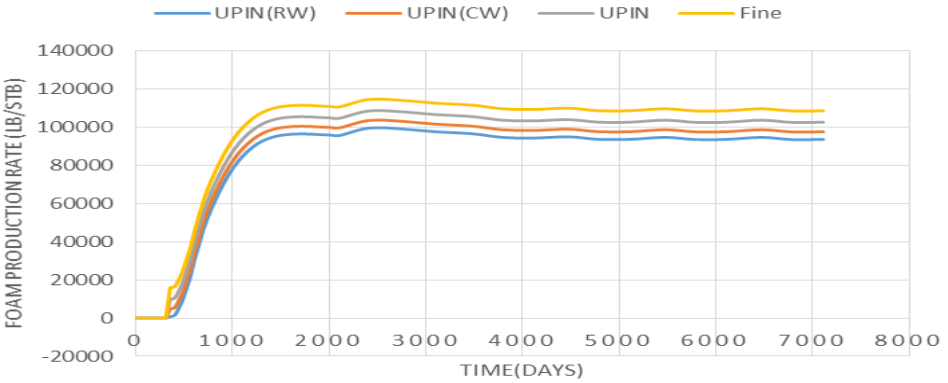

Figure 45. Foam Production Rate for Fractured Reservoir

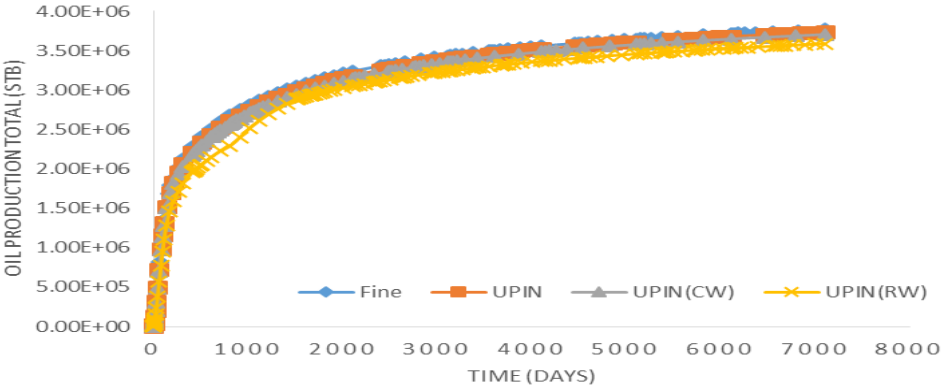

Figure 46. Oil Production Total for Fractured Reservoir

Table 11. Comparison of Different Scenarios in aspect of CPU Time

	UPIN	UPIN(CW)	UPIN(RW)
Reservoir with one injection and Production Well	7.2 times faster than fine model	6.13 times faster than fine model	5.62 times faster than fine model
5-Spot	8.82	6.24	5.62
Fractured Reservoir	4	3.69	3.52

Table 12. Comparison of Different Scenarios in aspect of Foam Adsorption Total (Percentage Error)

	UPIN	UPIN(CW)	UPIN(RW)
Reservoir with one injection and Production Well	3.1432%	3.1433%	4%
5-Spot	0.29%	0.96%	9%
Fractured Reservoir	3.21%	6.43%	9.65%

Table 13. Comparison of Different Scenarios in aspect of Foam Decay (Percentage Error)

	UPIN	UPIN(CW)	UPIN(RW)
Reservoir with one injection and Production Well	3.539%	6.193%	7%
5-Spot	0.03	0.06	0.09%
Fractured Reservoir	3.508%	7.017%	10.526%

Table 14. Comparison of Different Scenarios in aspect of Foam in Solution (Percentage Error)

	UPIN	UPIN(CW)	UPIN(RW)
Reservoir with one injection and Production Well	2.27%	5.307%	10.365%
5-Spot	0.35%	5.131%	23.34%
Fractured Reservoir	1.59%	3.18%	6.17%

Table 15. Comparison of Different Scenarios in aspect of Foam Production Rate (Percentage Error)

	UPIN	UPIN(CW)	UPIN(RW)
Reservoir with one injection and Production Well	0.37%	3.048%	6.086%
5-Spot	1.92%	2.62%	26.67%
Fractured Reservoir	4.27%	9.61%	16.02%

Table 16. Comparison of Different Scenarios in aspect of Oil Production Total (Percentage Error)

	UPIN	UPIN(CW)	UPIN(RW)
Reservoir with one injection and Production Well	0.83%	1.69%	4.82%
5-Spot	0.58%	0.95%	9.66%
Fractured Reservoir	0.83%	1.75%	4.89%

9. SUMMERY OF RESULTS

Chemical enhance oil recoveries processes are extremely complex processes with very high computing volumes. The high amount of computations can increase simulation time. The scale enhancement method defined in this study is a nature-based approach whose performance is based on the behavior of the flow lines. It was able to scale-up three-dimensional heterogeneous reservoir by maintaining accuracy and increasing the speed of simulation. Due to the high flexibility of this method, it is possible to simulate thermal processes with this method. The use of unstructured grid modeling was another achievement of this study, which allowed the definition of hybrid geometry, but in hybrid geometry, the accuracy and speed of simulation due to the conversion of various parameters such as transmissibility calculation (appendix) is low.

Future Work

Inspired By Nature Upscaling and Simulation of Steam Injection in Hydrocarbon Reservoirs

10. Appendix

One advantage of an unstructured grid is that it easily allows the use of composite grids consisting of geometries and topologies that vary throughout the model. In order to clarify hybrid grid simulation need to discuss the significant parameter that is transmissibility in Cartesian and radial geometry.

10.1. Cartesian Transmissibility Calculations

10.1.1. Block Center Transmissibility Calculations

10.1.1.1. X- Transmissibility

$$TRANX_i = \frac{CDARCY.TMLTX_i.A.DIPC}{B}$$

Where

$TRANX_i$: Transmissibility between cell i and cell j, its neighbor in the positive X-direction
CDARCY: Darcy's Constant
=0.00852702 (Metric)
= 0.00112712(Field)
= 3.6(Lab)
$TMLTX_i$: Transmissibility for cell i
A: Interface area between cell i and j
DIPC: Dip Correction

$$A = \frac{DX_j.DY_i.DZ_i.RNTG_i + DX_i.DY_j.DZ_j.RNTG_j}{DX_i + DX_j}$$

$$B = \frac{\left(\frac{DX_i}{PERMX_i} + \frac{DX_j}{PERMX_j}\right)}{2}$$

$$DIPC = \frac{DHS}{DHS + DVS}$$

$$DHS = \left(\frac{DX_i + DX_j}{2}\right)^2$$

$$DVS = [DEPTH_i - DEPTH_j]^2$$

RNTG: is the net to gross ratio, which appears in the X- and Y-transmissibilities but not in the Z-transmissibility.

10.1.1.2. Y- Transmissibility

The expression for the Y-transmissibility value is entirely analogous to the above.

10.1.1.3. Z- Transmissibility

$$TRANZ_i = \frac{CDARCY.TMLTZ_i.A}{B}$$

Where

$TRANZ_i$: Transmissibility between cell i and cell j, its neighbor in the positive Z-direction that is below cell i .
$TMLTZ_i$: The Z-transmissibility for cell i

$$A = \frac{DZ_j.DX_i.DY_i + DZ_i.DX_j.DY_j}{DZ_i + DZ_j}$$

$$B = \frac{\left(\frac{DZ_i}{PERMZ_i} + \frac{DZ_j}{PERMZ_j}\right)}{2}$$

There is no dip correction in the z-transmissibility.

10.2. Radial Transmissibility Calculations

10.2.1. R-Transmissibility

$$TRANR_i = \frac{CDARCY.TMLTR_i.DIPC}{\frac{1}{T_i}+\frac{1}{T_j}}$$

Where

$$T_i = \frac{PERMR_i.RNTG_i.D\theta_i.DZ_i}{D_{1P}}$$

$$D_{1P} = \frac{R_1^2}{(R_2^2-R_1^2)}\ln\left(\frac{R_1}{R_2}\right) + \frac{1}{2}$$

$$T_j = \frac{PERMR_j.RNTG_j.D\theta_j.DZ_j}{D_{2M}}$$

$$D_{2M} = \frac{R_3^2}{(R_3^2-R_2^2)}\ln\left(\frac{R_3}{R_2}\right) - \frac{1}{2}$$

R_1: is the inner radius of cell i,
R_2: is the outer radius of cell i,
R_3: is the outer radius of cell j,

$$DIPC = \frac{DHS}{DHS+DVS}$$

Where

$$DHS = (\frac{1}{2}(R_3 - R_1))^2$$

$$DVS = (DEPTH_i - DEPTH_j)^2$$

10.2.2. Azimuthal Transmissibility

$$TRANT_i = \frac{CDARCY.TMLTT_i.DIPC}{\frac{1}{T_i}+\frac{1}{T_j}}$$

Where

$$T_i = \frac{2.PERMT_i.RNTG_i.DZ_i.\ln(\frac{R_2}{R_1})}{D\theta_i}$$

R_1: is the inner radius
R_2: is the outer radius

$$DIPC = \frac{DHS}{DHS+DVS}$$

$$DHS = (\frac{1}{2}(D\theta_i + D\theta_j).R_{mean})^2$$

$$DVS = (DEPTH_i - DEPTH_j)^2$$

R_{mean}: Represents an average of the inner and outer radius

10.2.3. Vertical Transmissibility

$$TRANZ_i = \frac{CDARCY.TMLTZ_i}{\frac{1}{T_i}+\frac{1}{T_j}}$$

Where

$T_i = \frac{PERMZ_i.D\theta_i.(R_2^2-R_1^2)}{DZ_i}$

R_1: is the inner radius
R_2: is the outer radius

10.3. Well Inflow Performance

$$q_{P,j} = T_{w,j}M_{P,j}\left(P_j - P_w - H_{wj}\right)$$

Where

$q_{P,j}$: Volumetric flow rate of phase p in connection j
$T_{w,j}$: Connection transmissibility factor
$M_{P,j}$: The phase mobility at the connection
P_j: Nodal pressure in the grid block containing the connection
P_w: Bottom hole pressure of the well
H_{wj}: Wellbore pressure head between the connection and the well's bottom hole datum depth

10.3.1. Connection Transmissibility Factor in Radial Grids ($T_{w,j}$)

$$T_{w,j} = \frac{c\theta Kh}{\frac{r_2^2}{r_2^2-r_w^2}\ln(r_2/r_w)-0.5+S}$$

θ: is the segment angle of the grid block in radian
r_2: is the block's outer radius
c: is unit conversion factor , 0.001127 in the field unit
Kh: Effective permeability times net thickness of the connection
r_w: is the wellbore radius
S: is the skin factor

In hybrid grid simulation (Radial-Cartesian) at the common boundary of these two types of cells, the following transformations are performed during simulation calculations:

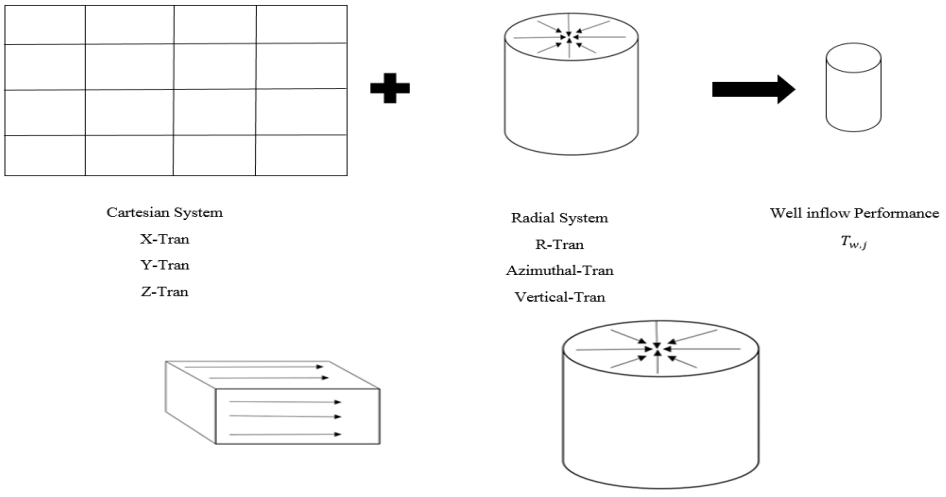

Figure 48. Linear and Radial Flow Regime

REFERENCES

[1] Mohammad Reza Rasaei, Muhammad Sahimi, "Upscaling and Simulation of Waterflooding in Heterogeneous Reservoirs Using Wavelet Transformations: Application to the SPE-10 Model, 20 July 2007.

[2] Masoud Babaei, Multiscale Wavelet and Upscaling-Downscaling for Reservoir Simulation, January 2013.

[3] An Introduction to Reservoir Simulation Using MATLAB, SINTEF ICT, Department of Applied Mathematics , May 27, 2014 Oslo, Norway.

[4] F. Brezzi and M. Fortin. Mixed and Hybrid Finite Element Methods, volume 15 of Springer Series in Computational Mathematics. Springer Verlag, New York, 1991. ISBN 0-387-97582-9.

[5] J. E. Aarnes, S. Krogstad, and K.-A. Lie. Multiscale mixed/mimetic methods on corner-point grids. Comput. Geosci., 12(3):297-315, 2008. ISSN 1420-0597.

[6] F. Brezzi, K. Lipnikov, and V. Simoncini. A family of mimetic finite difference methods on polygonial and polyhedral meshes. Math. Models Methods Appl. Sci., 15:1533-1553, 2005.

[7] M. A. Christie and M. J. Blunt. Tenth SPE comparative solution project: A comparison of upscaling techniques. SPE Reservoir Eval. Eng., 4:308-317, 2001.

[8] Y. Efendiev and T. Y. Hou. Multiscale Finite Element Methods, volume 4 of *Surveys and* Tutorials in the Applied Mathematical Sciences. Springer Verlag, New York, 2009.

[9] D. W. Peaceman. Fundamentals of Numerical Reservoir Simulation. Elsevier Science Inc., New York, NY, USA, 1991. ISBN 0444415785.

[10] D. K. Ponting. Corner point geometry in reservoir simulation. In P. King, editor, Proceedings of the 1st European Conference on Mathematics of Oil Recovery, Cambridge, *1989*, pages 45-65, Oxford, July 25-27 1989. Clarendon Press.

[11] M. Prevost, M. Edwards, and M. Blunt. Streamline tracing on curvilinear structured and unstructured grids. *SPE J.*, 7(2):139-148, June 2002.

[12] Aasum, Y., Kasap, E., Kelkar, M.: "Analytical Upscaling of Small-Scale Permeability Using a Full Tensor", Paper SPE 25913 presented at the SPE Rocky Mountain Regional/Low Permeability Reservoirs Symposium held in Denver, CO, April 12-14, 1993.

[13] Barker, J.W., Thibeau, S.: "A Critical Review of the Use of Pseudo Relative Permeabilities for Upscaling", Paper SPE 35491 presented at European 3-D Reservoir Modeling Conference held in Stavanger, Norway, April 16-17, 1996.

[14] Bedrikovetsky, P.G., Potsch, K.T., Polyanin, A.D., Zhurov, A.I.: "Upscaling of the Water flood Reservoir Properties on the Core Level: Laboratory Study, Macro and Micro Modeling", Paper SPE 29870 presented for SPE Middle East Oil Show held in Bahrain, March 11-14, 1995.

[15] Coll, C., Muggeridge, A.H., Jing,, X.D.: "Regional Upscaling: A New Method to Upscale Waterflooding in Heterogeneous Reservoirs for a Range of Capillary and Gravity Effects", Paper SPE 59337 presented at 2000 SPE/DOE Improved Oil Recovery Symposium held in Tulsa, OK, April 3-5, 2000.

[16] Craft, B.C., Hawkins, M.F.: Applied Reservoir Engineering, Prentice Hall, 1990.

[17] Vladimir Alvarado and Eduardo Manrique , "Enhanced Oil Recovery: An Update Review" , Department of Chemical and Petroleum Engineering, University of Wyoming, Department 3295,1000 E. University Ave, Laramie, WY, USA .

[18] Crowe, C. M. and Nishio, M. Convergence Promotion in the Simulation of Chemical Processes - The General Dominant Eigenvalue Method.

[19] Van Poolen H.K "Fundamental of EOR", Chapter 5, Penwell Books, Tulsa, 1980.

[20] Don W.Green, G.Paul Willhite, “Enhanced Oil Recovery”, Chapter 5, Socity of Petroleum Enginners Textbook Series Vol.6, 1998-2003.

[21] Faroug Ali, S.M. and Selby, Rawya J., “Function, Characteristics of EOR Foam Behavior Covered in Laboratory Investigations.” Technology, Oil and Gas Journal, (Feb.3, 1986) pp 57, 60-63.